RSC Advances

PAPER

View Article Online
View Journal | View Issue

Cite this: *RSC Adv.*, 2023, **13**, 17155

Electrochemical degradation of acrylic acid using $Ti/Ta_2O_5–IrO_2$ electrode

Jinrui Liu, Xiangxin Meng, Luwei Zhai, Guangfei Gao, Wenqiang Jiang and Xuan Zhang *

Received 27th March 2023
Accepted 21st May 2023

DOI: 10.1039/d3ra01997g

rsc.li/rsc-advances

Acrylic acid (AA) is widely used as a raw material in the industrial production of various chemicals. Its extensive use has produced environmental problems that need to be solved. The $Ti/Ta_2O_5–IrO_2$ electrode, a type of dimensionally stable anode, was used to investigate the electrochemical deterioration of AA. X-ray diffraction (XRD) and scanning electron microscopy (SEM) analysis showed that IrO_2 existed as an active rutile crystal and as a $TiO_2–IrO_2$ solid solution in $Ti/Ta_2O_5–IrO_2$ electrode with a corrosion potential of 0.212 V and chlorine evolution potential of 1.30 V. The effects of current density, plate spacing, electrolyte concentration, and initial concentration on the electrochemical degradation of AA were investigated. Response surface methodology (RSM) was used to determine the ideal degradation conditions: current density 22.58 mA cm^{-2}, plate spacing 2.11 cm, and electrolyte concentration 0.07 mol L^{-1}, and the highest degradation rate reached was 95.6%. Free radical trapping experiment verified that reactive chlorine played a dominant role in the degradation of AA. The degradation intermediates were analyzed by GC-MS.

1. Introduction

As an extremely important basic processing raw material and intermediate in today's chemical industry, AA has highly active polar molecules, unsaturated double bonds, and a carboxylic acid structure.[1] Many kinds of polymers can be prepared by polymerization, crosslinking, and copolymerization of AA. It is widely used in many industrial fields, such as rubber,[2] paint,[3] plastic,[4] adhesive,[5] flocculant,[6] synthetic fiber,[7] leather processing,[8] superabsorbent resin[9], and nano composite materials.[10] The global AA market reached $12 billion in 2020 and is expected to reach $19.2 billion in 2030. AA is the main basic component of absorbent polymers. The increasing demand for superabsorbent polymers and the widespread acceptance of acrylic-based products in emerging economies, such as the Asia-Pacific region, has been driving the development of the AA market.[11]

With vigorous industrial development, the supply of AA is increasing year by year. In the process of expanding the production scale, a large amount of AA wastewater is produced. Monomer AA has a strong irritating effect on the respiratory tract and eyes, and its highly corrosive property can burn the skin[12]. The huge pollution risk has caused a series of environmental problems. For the use of AA, strict government regulations have been implemented in North America and Europe.[13]

In recent years, China has the world's fastest-growing acrylic acid industry and at the same time, also produced a large amount of AA wastewater. This wastewater has high COD concentration, high toxicity, poor biodegradability, slow degradation rate in the natural environment, irritating odor, corrosive, moderate toxicity, *etc.*[14] The harmless treatment of AA wastewater has become one of the important factors that restrict the sustainable development of AA industry.

Incineration is often used in industry to remove highly concentrated AA wastewater. However, this method consumes a lot of energy and increases the economic cost. Adding chemicals by chemical treatment will produce by-products of chemical sludge, which needs to be properly treated and disposed of.[13] Especially in some cities, chemical sludge is defined as hazardous waste and must be further treated for safe disposal.[15] Although the cost of the biological method is low, microorganisms cannot tolerate high concentration of AA wastewater.[16] Studies on the biodegradation of AA have shown that the mixed microbial community of activated sludge often needs to be pre-treated or diluted in advance when treating AA wastewater,[17] resulting in complex processes.[18]

Compared with other water treatment methods, electrochemical oxidation has the advantages of no secondary pollution and easy automatic control. It is widely used to treat all kinds of wastewater with high concentration, poor biodegradability, and difficult degradation.[19] Rajkumar *et al.* used $Ti/RuO_2–IrO_2$ electrodes to treat dye wastewater, and the degradation rates of COD and TOC were 73.5% and 32.8%, respectively, under optimal conditions.[20] Malpass *et al.* used $Ti/RuO_2–IrO_2–SnO_2$ electrodes to electrolyze pesticide wastewater, and the maximum removal rate of TOC reached 46%.[21] Makgae *et al.* used $Ti/Ta_2O_5–IrO_2$ electrode to degrade phenol, and the phenol degradation rate

School of Environmental Science and Engineering, Qilu University of Technology (Shandong Academy of Sciences), Jinan 250353, P. R. China. E-mail: zx@qlu.edu.cn

reached 100% after 2 h.[22] Dimensionally Stable Anode (DSA) is not prone to pollution and is the "heart" of electrocatalytic oxidation.[23] Commonly used substrate metal materials with strong corrosion resistance include Au, Pt, Ti, stainless steel, *etc.* Coatings consist of one or more transition metal oxides,[24,25] such as RuO_2, IrO_2, SnO_2, TiO_2, PbO_2, MnO_2, and Ta_2O_5. Due to its excellent performance, DSA has been widely used in the fields of water electrolysis,[26,27] chloralkali process,[28,29] and sewage treatment.[30,31] Among them, Ti/Ta_2O_5–IrO_2 electrode has become a research hotspot for electrochemical oxidation because of its good electrocatalytic performance and chemical stability.[32] DSA has been proven to be an effective electrode for producing active chlorine, exhibiting higher removal efficiency in Cl^- medium compared with other electrolytes.[33]

In this study, Ti/Ta_2O_5–IrO_2 was used as the anode, and NaCl was used as the electrolyte to oxidise AA by producing active chlorine with strong oxidation in the electrolysis process. The Ti/Ta_2O_5–IrO_2 electrode was characterized by SEM and XRD, and CV and LSV curves were analyzed. The effects of current density, plate spacing, electrolyte concentration, and initial concentration of AA on the degradation of AA were investigated. The electrochemical degradation conditions were optimized by RSM. The degradation mechanism of AA was investigated by a free radical trapping experiment. The degradation intermediates of AA were analyzed by GC-MS. The electrochemical degradation pathway of acrylic acid was proposed.

2. Materials and methods

2.1. Experimental materials

AA ($C_3H_4O_2$) was purchased from Shanghai Macklin Biochemical Co., Ltd. Methanol (Damao, Tianjin, China) was HPLC grade. NaCl (Hushi, Taicang, China), H_3PO_4 (Fuyu, Tianjin, China), and NH_4F (Xiongda, Chengdu, China) were all AR grade.

The Ti/Ta_2O_5–IrO_2 anode (100 mm × 50 mm × 1 mm) prepared by conventional thermal decomposition and the Ti cathode were bought from Suzhou Shuertai Industrial Technology Co., Ltd (Suzhou, China).

2.2. Experimental methods

The experimental device was a 500 mL quartz electrolytic cell with 450 mL of AA solution (0.25, 0.50, 0.75, 1.00, 1.25 g L^{-1}). Current density (12, 16, 20, 24, 28 mA cm^{-2}), plate spacing (1, 2, 3, 4 cm), and electrolyte concentration (0.020, 0.035, 0.050, 0.065, 0.080 mol L^{-1}) were used as single factor variables. The magnetic stirrer was used to stir continuously throughout the process, and the samples were taken every 20 min. After filtering with a 0.22 μm filter, the samples were stored in disposable sampling tubes until analysis.

2.3. Analytical methods

The surface morphology of the Ti/Ta_2O_5–IrO_2 electrode was observed by SEM (mira 4, TESCAN, Czechoslovakia). Elemental analysis of the surface coating was performed by energy dispersive spectroscopy (EDS, GENESIS XM, EDAX Inc., USA). The crystal structure was determined by XRD (Ultima IV, Rigaku, Japan). Linear sweep voltammetry (LSV), cyclic voltammetry (CV), and Tafel curves were tested using an electrochemical workstation (CHI 660C, China Instrument, Shanghai, China) in 0.05 mol L^{-1} NaCl electrolyte. The working electrode and the counter electrode were the Ti/Ta_2O_5–IrO_2 electrode and platinum sheet electrode and the dimension was 10 mm × 10 mm × 1 mm. The reference electrode was a saturated Ag–AgCl electrode.

The degradation rate of AA was analyzed by high performance liquid chromatography (HPLC, LC-10AT, Shimadzu, Japan). The mobile phase was methanol : water (0.1% H_3PO_4 aqueous solution) = 30 : 70% at a flow rate of 1.0 mL min^{-1} and a wavelength of 220 nm.

Total organic carbon (TOC) was determined by a TOC analyzer (TOC-L CPH, Shimadzu, Japan). The reaction intermediates of AA were detected by gas chromatography mass spectrometry (GC-MS, QP2020, Shimadzu, Japan).

Using an HP-5MS column (30 m × 0.25 μm), the heating program was set to 50 °C at an initial temperature of 2 °C for 2 min, then at 5 °C min^{-1} to 100 °C for 10 min, and at 15 °C min^{-1} to 295 °C for 10 min. Electronic pressure control was set to a constant current mode with vacuum compensation. The helium flow rate was set to 1.2 mL min^{-1}. Ions were produced by electron ionization (EI) (electron energy 70 eV) in the ionization chamber of a mass spectrometer. The mass spectrometer scanned from $m/z = 20$ to $m/z = 800$ with a cycle time of 1 s.

3. Results and discussion

3.1. Electrode morphology and electrochemical analysis

EDS (Fig. 1a) clearly showed the diffraction peaks of elements Ta, Ir, O, and Ti, whose weight percentages were 45.6, 32.7, 15.9, and 5.8%, respectively. Fig. 1b shows the SEM image of the unused Ti/Ta_2O_5–IrO_2 electrode, which had a uniform distribution of grains on the electrode surface and was considered as active rutile IrO_2 by Babaei *et al.*[34] The Ta_2O_5–IrO_2 coating was evenly covered on the Ti matrix. The Ir element was helpful in binding the coating to the substrate more closely, which could not only prevent the corrosion of pollutants on the Ti matrix, but also prevent contact between high-valence state metals and the Ti matrix in the electrolytic process.[35] The above results showed that Ir and Ta were well mixed on the surface, and the plate had good electrocatalytic performance. However, after 100 h of use (Fig. 1c), it could be seen that the sharpness of IrO_2 grains slightly became smaller. The surface coating was clearly adhered to with contaminants. The experiment showed that there was a significant effect on the distribution of grains on the electrode surface, thus confirming the catalytic activity of the electrode.

As can be seen from the XRD pattern (Fig. 2a), the main diffraction peaks corresponded to Ti, IrO_2, and TiO_2–IrO_2. Each diffraction peak was sharp and the intensity was high, indicating a good crystallinity of the sample. Among them, the diffraction peak of Ti was the strongest, which was mainly because the Ti matrix was detected by the thin coating. The absence of TiO_2 diffraction peaks indicated that the Ti matrix was not oxidized, which meant that the coating had adhesion

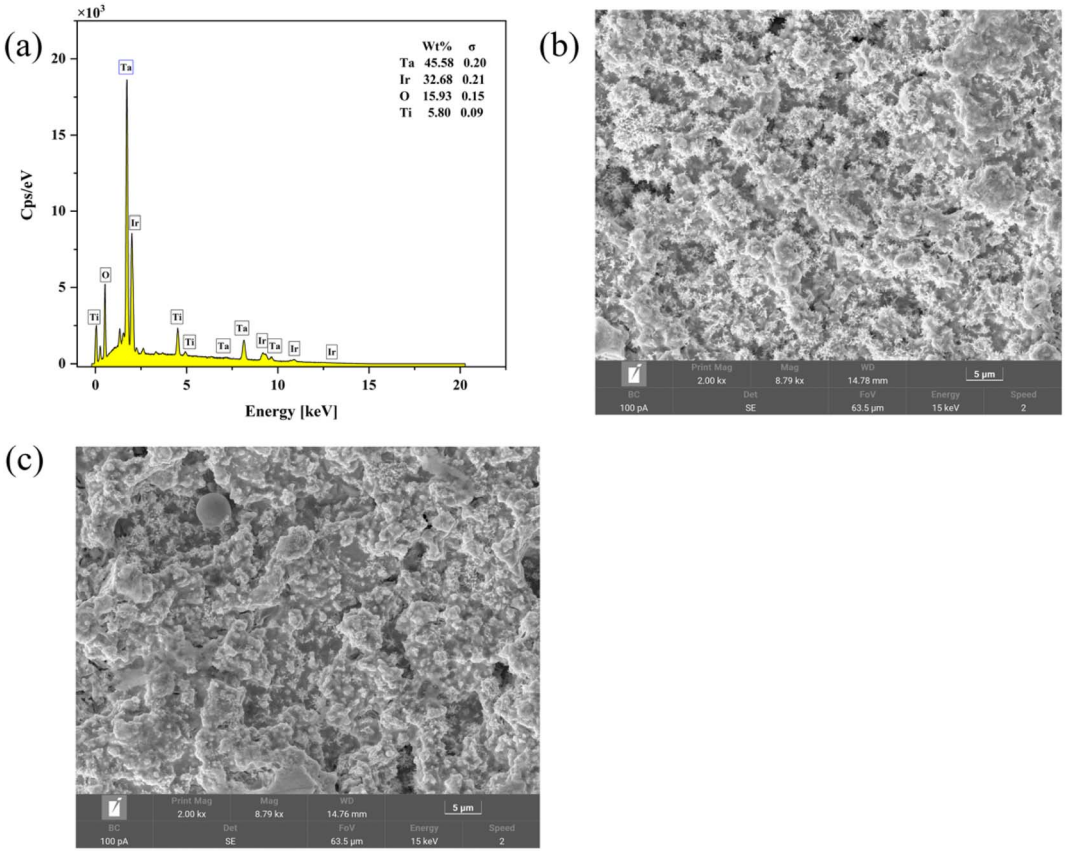

Fig. 1 EDS (a) and SEM ((b) before use, (c) after use) pattern of the Ti/Ta_2O_5–IrO_2 electrode.

and durability. Since the atomic radii of Ir^{4+} and Ti^{4+} were very similar, and TiO_2 and IrO_2 were both rutile-type semiconductor oxides with certain solubility, TiO_2–IrO_2 solid solution could be formed.[36] The surface of the anode coating was mainly composed of IrO_2 crystal and TiO_2–IrO_2 solid solution. When IrO_2 is dissolved in Ta^{5+}, the IrO_2 cell expanded, increasing the intensity of the TiO_2 diffraction peak. The performance of the plate's electrocatalytic system was significantly influenced by the miscibility of Ir and Ta, which was influenced by changes in the size of the IrO_2 unit cell.[37] There was no Ta_2O_5 diffraction peak in XRD, indicating that Ta_2O_5 existed in an amorphous form in the coating. Ta_2O_5, an inert oxide, could enhance the durability and stability of IrO_2 as well as prevent its dissolution in acidic environments. In addition, it could also enhance the anode's ability to resist the passivation of precipitated oxygen.[38] Therefore, their compatibility was crucial to increasing the durability of the coating.

As shown by the Tafel curve in Fig. 2b, Ti/Ta_2O_5–IrO_2 has a corrosion potential of 0.212 V (Fig. 2b) and a chlorine evolution potential of 1.30 V (Fig. 2c). The lower chlorine evolution potential increased the production of active chlorine. Therefore, the relatively low chlorine evolution potential of the Ti/Ta_2O_5–IrO_2 electrode also reflected its good performance. Fig. 2d shows the CV curves of the Ti/Ta_2O_5–IrO_2 electrode in the low potential region from −0.5 V to +1.28 V. The images showed a good closure and a large effective area, indicating that the electrochemical activity of the Ti/Ta_2O_5–IrO_2 electrode was great, consistent with the results in Fig. 1b.

3.2. Effect of single factors on AA degradation

Current density is the main parameter to measure the production rate of strong oxidizing free radicals on the electrode surface and the energy consumption in the electrocatalytic process. The increase in current density can effectively promote the generation and transfer of electrons. Fig. 3a displays the relationship between current density and the reaction rate constant (Ka). With the increase in current density, the degradation rate of AA increased and the Ka increased from 0.01026 min^{-1} to 0.03744 min^{-1}. However, when the current density reached 20 mA cm^{-2}, the increase in Ka was not obvious. This is because the high current density helps to produce free radicals that could be used for the electrochemical degradation of AA. But if the amount of generated free radicals is too high, it is difficult to react with pollutants around the electrode in time, leading to side reactions and thus reducing the utilization of free radicals.

The amount of electrolyte in the solution also has an impact on electron transfer. Therefore, the degradation rate did not increase significantly with the increase in current density. Wang's experiment[39] also confirmed that the increase in current density would lead to an increase in energy consumption. More energy would be consumed or converted into heat by side

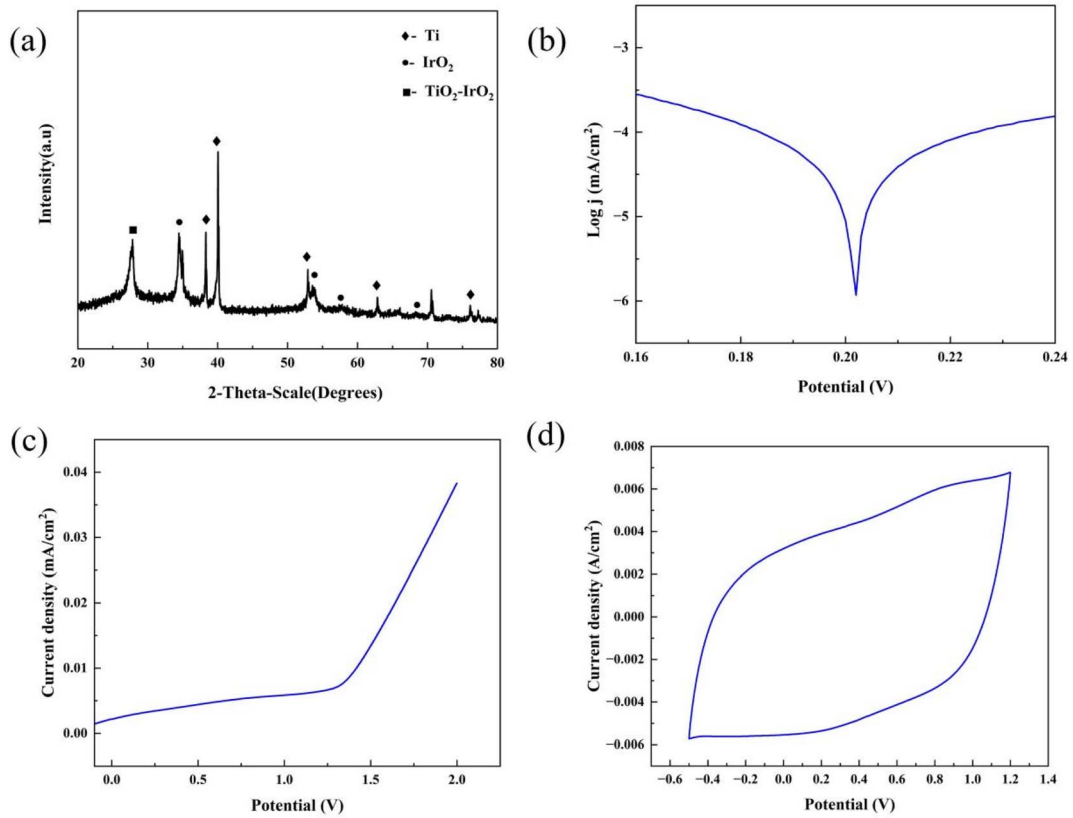

Fig. 2 XRD (a) pattern of the Ti/Ta_2O_5–IrO_2 electrode, Tafel (b), LSV (c), and CV (d) curves of the Ti/Ta_2O_5–IrO_2 electrode. LSV and CV were tested in 0.05 mol L^{-1} NaCl solution at a scan rate of 50 mV s^{-1}.

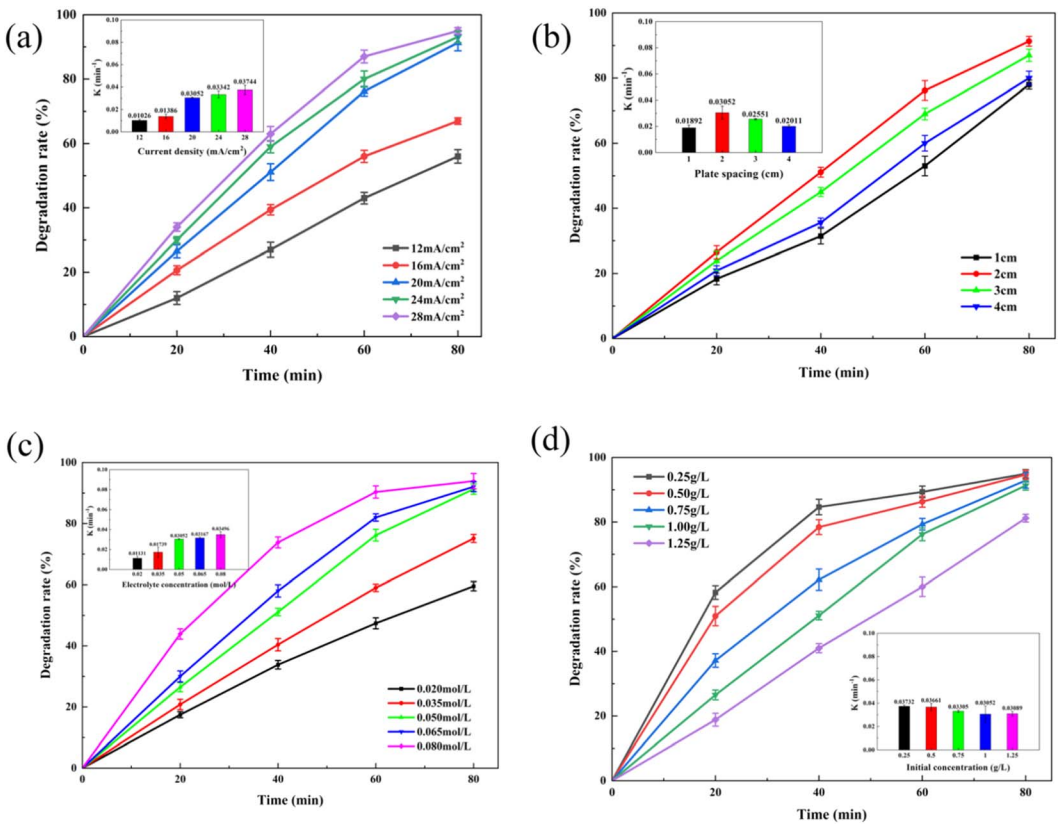

Fig. 3 Effects of current density (a), plate spacing (b), electrolyte concentration (c), and AA concentration (d) on AA degradation.

reactions.[40,41] In the electrochemical degradation process, pursuing high degradation rate would lead to excessive energy consumption. Therefore, it is not economical to pursue high degradation efficiency of AA only by increasing the current density. 20 mA cm^{-2} was chosen as the optimal current density.

Fig. 3b shows the influence of plate spacing on AA degradation. Ka varied between 0.01892 min^{-1} to 0.03052 min^{-1}. Ka reached its maximum value at a plate spacing of 2 cm. The various ions in the solution would move in a certain direction under the influence of the electric field as a result of the "electromigration" phenomenon, and the diffusion and convection of the solution components would occur. The components of the solution would diffuse and convect less as the distance between the plates grew.

Free radicals generated near the electrode would react slowly with organic matter in the solution, resulting in the degradation of AA. In addition, with the increase in plate spacing, the mass transfer resistance increases, resulting in a decrease in the degradation rate. At the same time, the increase in voltage between the electrodes led to energy consumption improvement. To maximize the degradation rate and minimize energy consumption, choosing a short electrode distance is advantageous. However, if the distance between the plates is too small, a short circuit may occur, and the anode surface is also easy to passivation and increase energy consumption. Besides, the solution is difficult to diffuse in a small space.[39–42] Therefore, 2 cm was chosen as the ideal plate spacing.

Electrolytes in the presence of electric current produce substances with oxidizing activity, which could promote or inhibit the degradation of organic matter.[43] The change in AA degradation rate is shown in Fig. 3c. The degradation rates of 0.05, 0.065, and 0.08 mol L^{-1} NaCl concentration all reached more than 90% in 80 min. The reaction process is shown in eqn (1)–(3). Cl^- produced active chlorine with strong oxidation in the presence of electric current,[44] which is commonly used for the treatment of refractory organic matter.[45]

The electrolyte concentration would affect the amount of generated active chlorine. In a certain concentration range, the higher the electrolyte concentration, the quicker the electron transfer rate and the more active chlorine produced, which was more conducive to the degradation of AA. However, when the electrolyte concentration is too high, a large amount of active chlorine is produced, which reduces the diffusion rate of AA and affect the reaction efficiency. Moreover, active chlorine could not react with AA completely, which would reduce the utilization rate of active chlorine.[39] When NaCl concentration exceeded 0.05 mol L^{-1}, the Ka did not increase significantly, so 0.05 mol L^{-1} NaCl was considered the optimal electrolyte concentration.

$$2Cl^- \rightarrow Cl_2 + 2e^- \quad (1)$$

$$Cl_2 + H_2O \rightarrow HClO + Cl^- + H^+ \quad (2)$$

$$HClO \rightarrow ClO^- + H^+ \quad (3)$$

The effect of the initial concentration of AA on the electrochemical degradation is shown in Fig. 3d. The degradation effect of AA at an initial concentration of 0.25 g L^{-1} was the best, and the degradation efficiencies decreased gradually with the initial concentration increasing. The reason might be that the degradation rate of low concentration organic pollutants was faster than their diffusion rate to the electrode surface,[35,46] so they were rapidly degraded once they reached the electrode surface. The reaction of AA on the Ti/Ta_2O_5–IrO_2 anode at low concentrations was a diffusion-controlled reaction, which was consistent with Zhao *et al.*[47,48] As the initial acrylic acid

Table 1 Three factors and three levels of experimental design

		Level		
Factors	Code	−1	0	1
Current density (mA cm^{-2})	X_1	12	20	28
Electrolyte concentration (mol L^{-1})	X_2	0.02	0.05	0.08
Plate spacing (cm)	X_3	1	2	3

Table 2 Parameters of the designed model

Source	Sum of squares	Degree of freedom (df)	Mean square (MS)	*F*-value	*p*-value
Model	1073.54	9	119.28	32.75	<0.0001
X_1-current density	101.25	1	101.25	27.80	0.0012
X_2-electrolyte	365.72	1	365.72	15.75	<0.0001
X_3-plate spacing	0.0741	1	0.0741	0.0203	0.8906
X_1X_2	0.0324	1	0.0324	0.0089	0.9275
X_1X_3	40.32	1	40.32	11.07	0.0126
X_2X_3	3.08	1	3.08	0.8456	0.3884
X_1^2	160.43	1	160.43	44.05	0.0003
X_2^2	108.67	1	108.67	29.84	0.0009
X_3^2	236.54	1	236.54	64.94	<0.0001
Residual	25.50	7	3.64		
Lack of fit	15.32	3	5.11	2.01	0.2554
Pure error	10.18	4	2.54		
Cor total	1099.03	16			
$R^2 = 0.9768$	$R_{aj}^2 = 0.9470$				C.V.% = 2.26

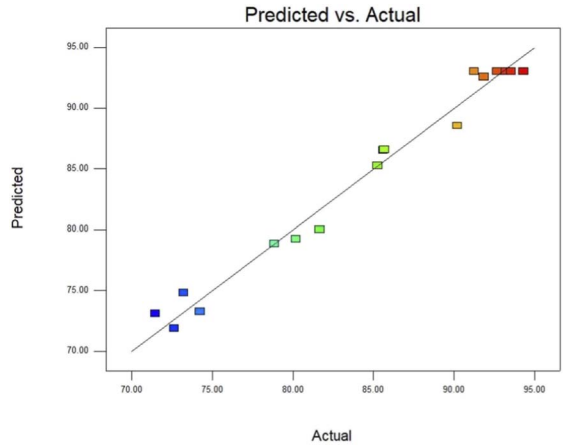

Fig. 4 The predicted and actual values of AA degradation rate.

concentration increased, more and more AA and intermediate products covered the electrode surface, preventing them from reacting with active chlorine. A large portion of active chlorine was consumed in the process, leading to a gradual decrease in the degradation rate.[41,46,49–51] The initial concentration increased from 0.25 g L^{-1} to 1.25 g L^{-1}, and the Ka value decreased from 0.03732 min^{-1} to 0.03039 min^{-1}, but the decrease was insignificant. It might be that the inhibitory effect of the produced intermediates on acrylic acid gradually reached its upper limit with increasing concentration. Furthermore, it is not practical to increase the degradation rate in practical engineering by blindly pursuing lower pollutant concentration. In this experiment, when the concentration exceeded 1 g L^{-1}, the degradation efficiency of AA was significantly reduced. Therefore, the initial AA concentration of 1 g L^{-1} was chosen.

3.3. Response surface methodology

3.3.1. Regression model and analysis of variance. The degradation rate of AA was used as the response index during the RSM process, which was conducted using the Design Expert 8.0 software. Based on the results of the single factor experiments (Table 1), a three-factor and three-level Box–Behnken design (BBD) method was used. The quadratic regression equation between current density (X_1), electrolyte concentration (X_2), plate spacing (X_3), and AA degradation rate (Y) was established:

$$Y = 93.41 + 3.56X_1 + 6.76X_2 + 0.0962X_3 + 0.0900X_1X + 3.18X_1X_3 + 0.8775X_2X_3 - 6.17{X_1}^2 - 5.08{X_2}^2 - 7.50{X_3}^2 \quad (4)$$

F-value and *p*-value in the variance analysis table could reflect the adequacy and significance of the RSM model. *F*-value is 32.75 and the *p*-value is less than 0.0001, indicating that the model is highly significant (Table 2). Obviously, $p = 0.2554$ indicated that the missing fit was not significant and the simulation was good. $R^2 = 0.9768$ demonstrated that this model could account for the change in AA degradation rate of 97.68%. The ${R_{aj}}^2 = 0.9470$ was very close to R^2, and C.V. = 2.26% was less than 10%, indicating that eqn (4) was highly accurate and reliable in predicting the degradation rate of AA.

According to the significance analysis of variables in the quadratic model, the order of significant influence of X_1, X_2, and X_3 on the electrochemical degradation of AA is as follows:

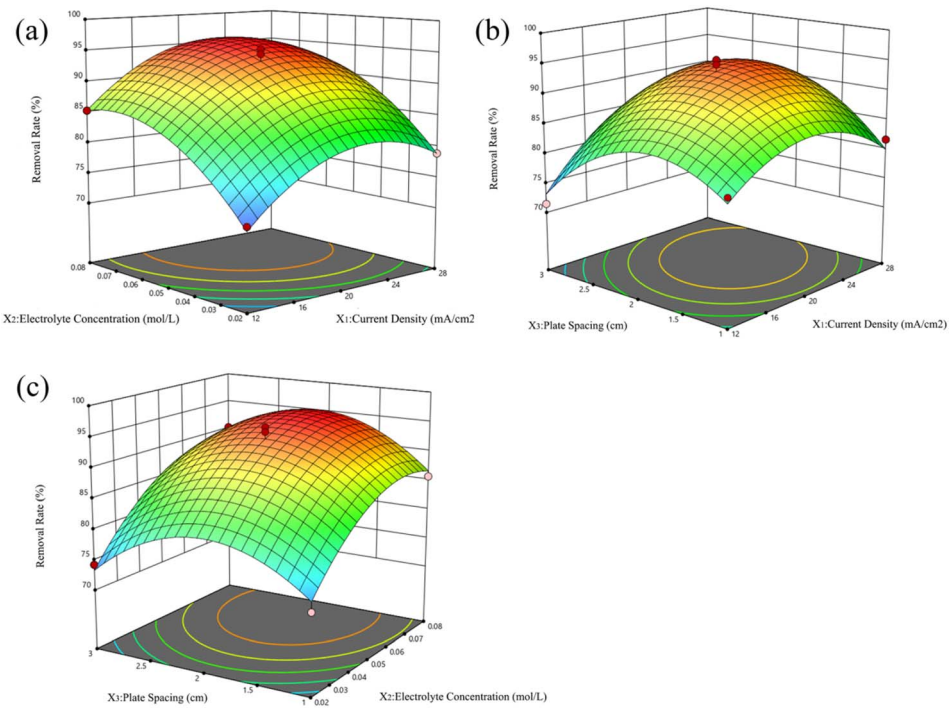

Fig. 5 Three-dimensional surfaces of the interaction of the independent variables: (a) for X_1 and X_3, (b) for X_1 and X_2, and (c) for X_2 and X_3.

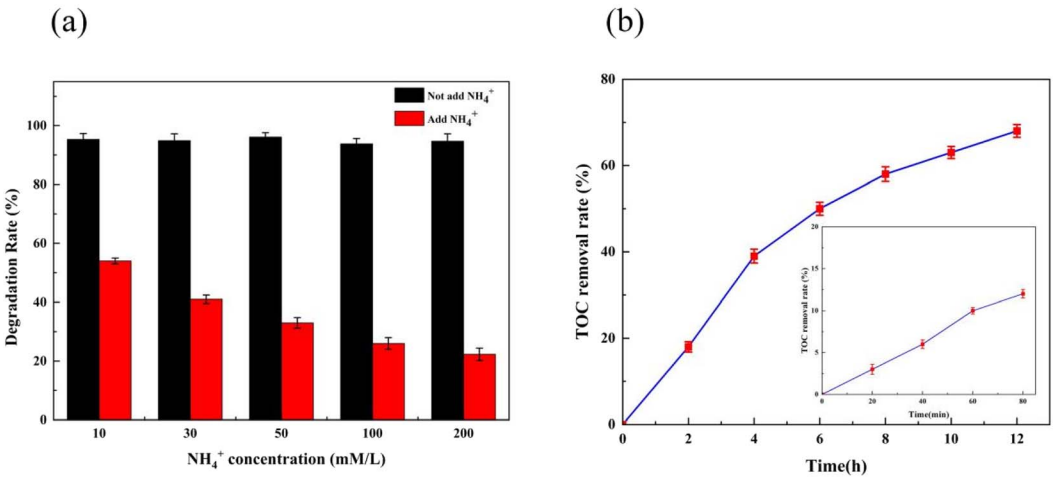

Fig. 6 Free radical trapping experiment (a) and TOC removal rate (b).

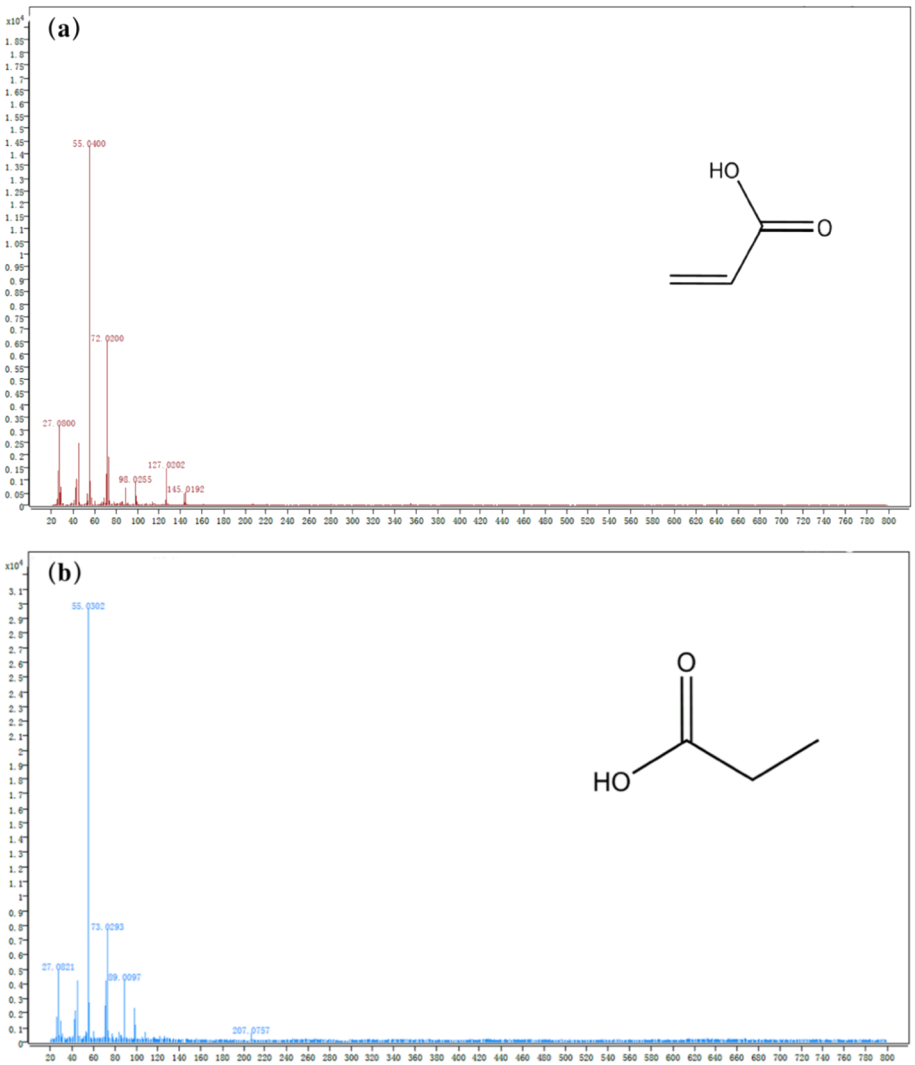

Fig. 7 EI spectra of before (a) and after (b) electrolysis.

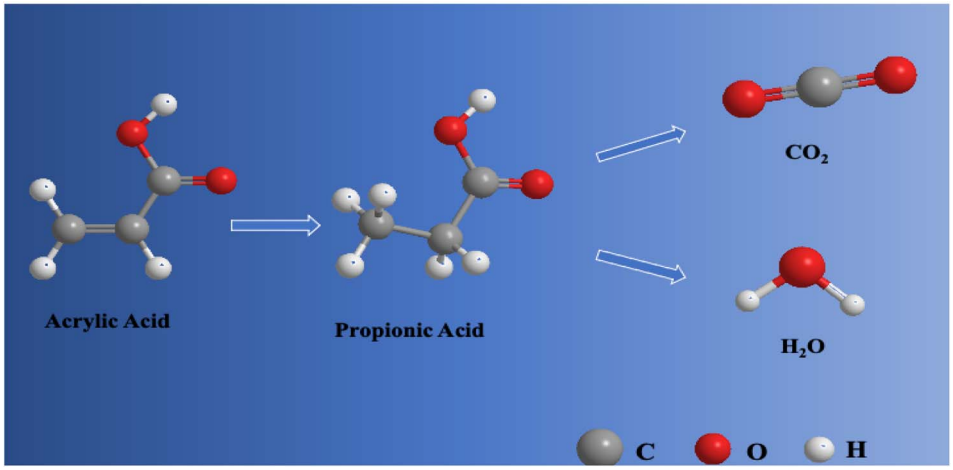

Fig. 8 Degradation mode of AA.

electrolyte concentration (X_2) > current density (X_1) > plate spacing (X_3). The interaction effect of X_1X_3 on the electrochemical oxidation degradation of AA was significant.

According to eqn (4) of the quadratic model, the AA degradation rate under each experimental condition could be predicted by the model (Fig. 4). Comparing the actual and predicted AA degradation rates, it could be seen that the predicted data and the experimental data are in good agreement with a straight line. Therefore, the quadratic regression model could be used to analyze and predict the degradation rate of AA by electrochemical oxidation technology under certain experimental conditions.

The 3D response surface diagrams (Fig. 5) show the independent effects and interactions of independent variables on dependent variables. Electrolyte concentration has a significant effect on the AA degradation rate. In contrast, the small significant effect of the plate spacing on the degradation rate might be due to the small gradient of the interval selected for the experiment.

According to the optimal conditions (current density 22.58 mA cm^{-2}, plate spacing 2.11 cm, NaCl concentration 0.07 mol L^{-1}) as determined by RSM, three parallel experiments were conducted. The average degradation rate of AA obtained was 95.6%, which was 4.3% higher than the previous one, indicating that the optimal condition calculated by the software was the optimal operating parameter.

3.4. Electrochemical degradation mechanism of AA

Due to the esterification reaction of AA with *tert*-butyl alcohol and methanol, ammonium was selected as the quenching agent.[52] With the increase in ammonium dosage (Fig. 6a), the degradation rate of AA decreased gradually. When the ammonium concentration increased to above 100 mM L^{-1}, the degradation rate of AA did not change significantly, indicating that active chlorine had been captured. At this time, the degradation rate of AA decreased by about 73.1%, indicating that reactive chlorine played a dominant role during the experiment.

After 80 min of reaction, the degradation rate of AA reached more than 95%, while the TOC removal rate was only about 12% (Fig. 6b), indicating that in this electrochemical system, AA might be converted to more antioxidant intermediates that were resistant to the electrochemically generated oxidants. Giraldo *et al.* proposed that incomplete mineralization of target contaminants could be attributed to the formation of refractory organic compounds in the presence of NaCl as a supporting electrolyte.[39,53] With increasing time, the intermediate products were further mineralized and the TOC decreased. The removal rate of TOC reached 72.92% after 12 h electrolysis.

The intermediates of AA degradation were identified by GC-MS. The substance at *m*/*z* 72.02 was AA prior to the reaction, according to EI analysis and database comparison (Fig. 7a), After electrolysis for 80 min under optimal conditions (Fig. 7b), the substance (*m*/*z* 73.0293) was determined to be propionic acid (CH_3CH_2COOH). The electrochemical degradation pathway of AA was deduced from the information on degradation products and combined with TOC removal in Fig. 8. AA was first reduced to propionic acid by breaking C=C, and propionic acid was then further oxidized to produce CO_2 and H_2O.

4. Conclusions

As a premium DSA electrode, Ti/Ta_2O_5–IrO_2 electrode has a dense surface structure and stable performance. IrO_2 was present in the electrode as an active rutile crystal, which joined with the Ti substrate to form a solid solution of TiO_2–IrO_2. Ta_2O_5 existed in an amorphous form, and IrO_2 cell was dissolved in Ta^{5+}. The reaction rate constant (Ka) increased from 0.01026 min^{-1} to 0.03744 min^{-1} when the current density was between 12 and 28 mA cm^{-2}. However, when the current density reached 20 mA cm^{-2}, the increase in reaction rate constant was not obvious. When the distance between the plates was 2 cm, the reaction rate constant (Ka) reached its maximum value.

In the range of 0.02–0.08 mol L^{-1} NaCl concentration, Ka increased from 0.01131 min^{-1} to 0.03496 min^{-1}, but the

increase of Ka was not obvious when the NaCl concentration exceeded 0.05 mol L^{-1}. With the increase in initial AA concentration, the degradation rate decreased gradually, but the degradation amount per unit time increased. Through RSM optimization experiments, the optimal reaction conditions were obtained: current density 22.58 mA cm^{-2}, plate spacing 2.11 cm, electrolyte concentration 0.07 mol L^{-1}. The degradation rate of AA reached 95.6% within 80 min, but it was not enough to mineralize AA completely. After 12 h, the TOC removal rate reached 72.92%, and the ideal mineralization effect was obtained. The free radical trapping experiment proved that active chlorine was the main oxidizing active substance and propanoic acid was formed during the degradation of AA.

Author contributions

J. L., data curation, writing—original draft; X. M., writing—review and editing; L. Z., data curation; G. G., supervision, validation; W. J., methodology. All authors have read and agreed to the published version of the manuscript.

Conflicts of interest

The authors declare that they have no known competing financial interests or personal relationships that could have appeared to influence the work reported in this paper.

Acknowledgements

This work was supported by the Natural Science Foundation of Shandong Province, China (ZR2020MB141).

References

1 M. Liu, X. Mao, H. Zhu, A. Lin and D. Wang, Water and corrosion resistance of epoxy–acrylic–amine waterborne coatings: Effects of resin molecular weight, polar group and hydrophobic segment, *Corros. Sci.*, 2013, **75**, 106–113.

2 S. Kocevski, S. Yagneswaran, F. Xiao, V. S. Punith, D. W. Smith and S. Amirkhanian, Surface modified ground rubber tire by grafting acrylic acid for paving applications, *Constr. Build. Mater.*, 2012, **34**, 83–90.

3 E. M. Dogan-Guner, S. Brownell, G. T. Schueneman, M. L. Shofner and J. C. Meredith, Enabling zero added-coalescent waterborne acrylic coatings with cellulose nanocrystals, *Prog. Org. Coat.*, 2021, **150**, 105969.

4 J. Sun, L. Yao, S. Sun, Z. Q. Gao and Y. P. Qiu, Effect of storage condition and aging on acrylic acid inverse emulsion surface-grafting polymerization of PET films initiated by atmospheric pressure plasmas, *Surf. Coat. Technol.*, 2011, **205**, 2799–2805.

5 G. C. Luque, R. Stürtz, M. C. G. Passeggi, L. M. Gugliotta, V. D. G. Gonzalez and R. J. Minari, New hybrid acrylic/collagen nanocomposites and their potential use as bioadhesives, *Int. J. Adhes. Adhes.*, 2020, **100**, 102624.

6 A. K. Sarkar, N. R. Mandre, A. B. Panda and S. Pal, Amylopectin grafted with poly (acrylic acid): development and application of a high performance flocculant, *Carbohydr. Polym.*, 2013, **95**, 753–759.

7 M. M. Hassan and K. Koyama, Multifunctional acrylic fibers prepared *via in situ* formed silver nanoparticles: Physicochemical, UV radiation protection, and antistatic properties, *Dyes Pigm.*, 2018, **159**, 517–526.

8 L. Peng, W. Long, W. Zhang and B. Shi, Leaching toxicity and ecotoxicity of tanned leather waste during production phase, *Process Saf. Environ. Prot.*, 2022, **161**, 201–209.

9 B. Rossi Canuto de Menezes, A. da Graça Sampaio, D. Morais da Silva, T. Larissa do Amaral Montanheiro, C. Yumi Koga-Ito and G. Patrocínio Thim, $AgVO_3$ nanorods silanized with γ-MPS: An alternative for effective dispersion of $AgVO_3$ in dental acrylic resins improving the mechanical properties, *Appl. Surf. Sci.*, 2021, **543**, 148830.

10 M. Shahzamani, S. Taheri, A. Roghanizad, N. Naseri and M. Dinari, Preparation and characterization of hydrogel nanocomposite based on nanocellulose and acrylic acid in the presence of urea, *Int. J. Biol. Macromol.*, 2020, **147**, 187–193.

11 Allied Market Research, *Market analytics: acrylic acid market: global size, trends and analysis report*, 2022, **https://www.alliedmarketresearch.com/acrylic-acid-market**.

12 S. X. Zhang, X. S. Chai and R. Jiang, Accurate determination of residual acrylic acid in superabsorbent polymer of hygiene products by headspace gas chromatography, *J. Chromatogr. A*, 2017, **1485**, 20–23.

13 J. Deng, L. Ren, Y. Pan, H. Gao and X. Meng, Antifungal property of acrylic denture soft liner containing silver nanoparticles synthesized *in situ*, *J. Dent.*, 2021, **106**, 103589.

14 L. Jin, Z. Luan, Y. Lian and Z. Ji, Pretreatment of acrylic fiber manufacturing wastewater by the Fenton process, *Desalination*, 2012, **284**, 62–65.

15 K. Y. Show, M. Ling, H. Guo and D. J. Lee, Laboratory and full-scale performances of integrated anaerobic granule-aerobic biofilm-activated sludge processes for high strength recalcitrant paint wastewater, *Bioresour. Technol.*, 2020, **310**, 123376.

16 J. Liang, Q. Wang, B. A. Yoza, Q. X. Li, C. Chen, J. Ming, J. Yu, J. Li and M. Ke, Rapid granulation using calcium sulfate and polymers for refractory wastewater treatment in up-flow anaerobic sludge blanket reactor, *Bioresour. Technol.*, 2020, **305**, 123084.

17 K. Y. Show, Y. G. Yan, J. Zhao, J. Shen, Z. X. Han, H. Y. Yao and D. J. Lee, Startup and performance of full-scale anaerobic granular sludge blanket reactor treating high strength inhibitory acrylic acid wastewater, *Bioresour. Technol.*, 2020, **317**, 123975.

18 M. H. Cui, L. Gao, H. S. Lee and A. J. Wang, Mixed dye wastewater treatment in a bioelectrochemical system-centered process, *Bioresour. Technol.*, 2020, **297**, 122420.

19 W. Wu, Z. H. Huang and T. T. Lim, Recent development of mixed metal oxide anodes for electrochemical oxidation of organic pollutants in water, *Appl. Catal., A*, 2014, **480**, 58–78.

20 D. Rajkumar and J. G. Kim, Oxidation of various reactive dyes with *in situ* electro-generated active chlorine for textile dyeing industry wastewater treatment, *J. Hazard. Mater.*, 2006, **136**, 203–212.

21 G. R. Malpass, D. W. Miwa, S. A. Machado, P. Olivi and A. J. Motheo, Oxidation of the pesticide atrazine at DSA electrodes, *J. Hazard. Mater.*, 2006, **137**, 565–572.

22 M. E. Makgae, M. J. Klink and A. M. Crouch, Performance of sol–gel titanium mixed metal oxide electrodes for electro-catalytic oxidation of phenol, *Appl. Catal., B*, 2008, **84**, 659–666.

23 N. N. Zhou, W. Zhang, J. L. Zhao, K. Li and S. B. Shen, DSA anode electric catalytic oxidation technology and research progress of phenol containing wastewater treatment, *Mod. Chem. Ind.*, 2017, **37**, 29–32.

24 T. C. M. Nonato, A. A. A. Alves, W. Broock, R. L. Dalsasso and M. L. Sens, The optimization of the electroflotation process using DSA electrodes for treating the simulated effluent of produced water from oil production, *Desalin. Water Treat.*, 2017, **70**, 139–144.

25 S. Trasatti, Electrocatalysis: understanding the success of DSA, *Electrochim. Acta*, 2000, **45**, 2377–2385.

26 G. Givirovskiy, V. Ruuskanen, L. S. Ojala, M. Lienemann, P. Kokkonen and J. Ahola, Electrode material studies and cell voltage characteristics of the *in situ* water electrolysis performed in a pH-neutral electrolyte in bioelectrochemical systems, *Heliyon*, 2019, **5**, e01690.

27 N. Sánchez-Padilla, S. M. Montemayor and F. Varela, An easy route to synthesize novel Fe_3O_4@ Pt core-shell nanostructures with high electrocatalytic activity, *J. New Mater. Electrochem. Syst.*, 2012, **15**, 171–179.

28 M. S. Zafar, M. Tausif, Z. Zia-ul-Haq, M. Ashraf and S. Hussain, New development of anodic electro-catalyst for chlor-alkali industry, *Port. Electrochim. Acta*, 2016, **34**, 257–266.

29 V. Trieu, B. Schley, H. Natter, J. Kintrup, A. Bulan and R. Hempelmann, RuO_2-based anodes with tailored surface morphology for improved chlorine electro-activity, *Electrochim. Acta*, 2012, **78**, 188–194.

30 V. Montiel, V. Garcia-Garcia, J. Gonzalez-Garcia, J. R. Perez-Mallol and A. Aldaz, Viability of the electrochemical treatment of industrial effluents, *J. New Mater. Electrochem. Syst.*, 2000, **3**, 269–274.

31 K. Rathinakumaran and R. M. Meyyappan, Electrochemical degradation of dye effluents using mixed oxide coated DSA electrode-a kinetic study, *Int. J. Chem. Sci.*, 2015, **13**, 1401–1409.

32 O. Scialdone, S. Randazzo, A. Galia and G. Filardo, Electrochemical oxidation of organics at metal oxide electrodes: The incineration of oxalic acid at IrO_2–Ta_2O_5 (DSA-O2) anode, *Electrochim. Acta*, 2009, **54**, 1210–1217.

33 M. G. Panizza, Direct and mediated anodic oxidation of organic pollutants, *Chem. Rev.*, 2009, **109**, 6541–6569.

34 T. Babaei, M. Zarei, M. G. Hosseini and M. M. Hosseini, Electrochemical advanced oxidation process of Phenazopyridine drug waste using different Ti-based IrO_2-Ta_2O5 anodes, *J. Taiwan Inst. Chem. Eng.*, 2020, **117**, 103–111.

35 Z. Yi, C. Kangning, W. Wei, J. Wang and S. Lee, Effect of IrO_2 loading on RuO_2–IrO_2–TiO_2 anodes: A study of microstructure and working life for the chlorine evolution reaction, *Ceram. Int.*, 2007, **33**, 1087–1091.

36 J. M. Hu, J. Q. Zhang and C. N. Cao, Thermolytic formation and microstructure of IrO_2 + Ta_2O_5 mixed oxide anodes from chloride precursors, *Thermochim. Acta*, 2003, **403**, 257–266.

37 M. Morimitsu, H. Tamura, M. Matsunaga and R. Otogawa, Polarization behaviour and lifetime of IrO_2–Ta_2O_5–SnO_2/Ti anodes in p-phenolsulfonic acid solutions for tin plating, *J. Appl. Electrochem.*, 2000, **30**, 511–514.

38 Y. E. Roginskaya, V. Morozova, E. N. Loubnin, A. V. Popov, Y. I. Ulitina and V. V. Z. a. S. A. lvanov, X-Ray diffraction, transmission electron microscopy and X-Ray photoelectron spectroscopic characterization of IrO_2 + Ta_2O_5 films, *J. Am. Chem. Soc.*, 1993, **89**, 1707–1715.

39 J. Wang, D. Zhi, H. Zhou, X. He and D. Zhang, Evaluating tetracycline degradation pathway and intermediate toxicity during the electrochemical oxidation over a Ti/Ti_4O_7 anode, *Water Res.*, 2018, **137**, 324–334.

40 L. Xu, Y. Xin and J. Wang, A comparative study on IrO_2–Ta_2O_5 coated titanium electrodes prepared with different methods, *Electrochim. Acta*, 2009, **54**, 1820–1825.

41 Q. Zhuo, J. Wang, J. Niu, B. Yang and Y. Yang, Electrochemical oxidation of perfluorooctane sulfonate (PFOS) substitute by modified boron doped diamond (BDD) anodes, *Chem. Eng. J.*, 2020, **379**, 122280.

42 M. Minakshi and M. Ionescu, Anodic behavior of zinc in Zn-MnO_2 battery using ERDA technique, *Int. J. Hydrogen Energy*, 2010, **35**, 7618–7622.

43 D. Jager, D. Kupka, M. Vaclavikova, L. Ivanicova and G. Gallios, Degradation of Reactive Black 5 by electrochemical oxidation, *Chemosphere*, 2018, **190**, 405–416.

44 Z. Frontistis and S. Meriç, The role of operating parameters and irradiation on the electrochemical degradation of tetracycline on boron doped diamond anode in environmentally relevant matrices, *J. Chem. Technol. Biotechnol.*, 2018, **93**, 3648–3655.

45 C. Y. Cheng and G. H. Kelsall, Models of Hypochlorite production in electrochemical reactors with plate and porous anodes, *J. Appl. Electrochem.*, 2007, **37**, 1203–1217.

46 S. Qian, S. Liu, Z. Y. Jiang, D. L. Deng, B. B. Tang and J. Z. Zhang, Electrochemical degradation of tetracycline antibiotics using a Ti/SnO_2-Sb_2O_3/PbO_2 anode: Kinetics, pathways, and biotoxicity change, *J. Electrochem. Soc.*, 2019, **166**, E192–E199.

47 H. Li, Q. Yu, B. Yang, Z. Li and L. Lei, Electrochemical treatment of artificial humidity condensate by large-scale boron doped diamond electrode, *Sep. Purif. Technol.*, 2014, **138**, 13–20.

48 R. Zhao, X. Zhang, F. L. Chen, X. B. Man and W. Q. Jiang, Study on electrochemical degradation of nicosulfuron by IrO_2-Based DSA electrodes: Performance, kinetics, and degradation mechanism, *Int. J. Environ. Res. Public Health*, 2019, **16**, 343–347.

49 L. A. Perea, R. E. Palma-Goyes, J. Vazquez-Arenas, I. Romero-Ibarra, C. Ostos and R. A. Torres-Palma, Efficient cephalexin

degradation using active chlorine produced on ruthenium and iridium oxide anodes: Role of bath composition, analysis of degradation pathways and degradation extent, *Sci. Total Environ.*, 2019, **648**, 377–387.

50 B. Garza-Campos, D. Morales-Acosta, A. Hernández-Ramírez, J. L. Guzmán-Mar, L. Hinojosa-Reyes, J. Manríquez and E. J. Ruiz-Ruiz, Air diffusion electrodes based on synthetized mesoporous carbon for application in amoxicillin degradation by electro-Fenton and solar photo electro-Fenton, *Electrochim. Acta*, 2018, **269**, 232–240.

51 Y. Yao, M. Li, Y. Yang, L. Cui and L. Guo, Electrochemical degradation of insecticide hexazinone with Bi-doped PbO(2) electrode: Influencing factors, intermediates and degradation mechanism, *Chemosphere*, 2019, **216**, 812–822.

52 L. Tian, M. Zhu, L.-S. Zhang, L.-J. Zhou, J.-P. Fan, D.-S. Wu and J.-P. Zou, New insights on the role of NaCl electrolyte for degradation of organic pollutants in the system of electrocatalysis coupled with advanced oxidation processes, *J. Environ. Chem. Eng.*, 2022, **10**, 107414.

53 A. L. Giraldo, E. D. Erazo-Erazo, O. A. Flórez-Acosta, E. A. Serna-Galvis and R. A. Torres-Palma, Degradation of the antibiotic oxacillin in water by anodic oxidation with Ti/IrO_2 anodes: Evaluation of degradation routes, organic by-products and effects of water matrix components, *Chem. Eng. J.*, 2015, **279**, 103–114.